Energy Conversion and Management 52 (2011) 2911–2918

Contents lists available at ScienceDirect

Energy Conversion and Management

journal homepage: www.elsevier.com/locate/enconman

Thermoelectric generator sandwiched in a crossflow heat exchanger with optimal connectivity between modules

Simon Bélanger, Louis Gosselin *

Département de génie mécanique, Université Laval, 1065, avenue de la Médecine, Québec City, QC, Canada G1V 0A6

ARTICLE INFO

Article history:
Received 29 April 2010
Accepted 28 February 2011
Available online 4 May 2011

Keywords:
Thermoelectric
Non-uniform
Genetic algorithm
Waste heat
Crossflow

ABSTRACT

The design of a thermoelectric generator sandwiched in the wall of a crossflow heat exchanger was optimized. A numerical model has been developed and validated. The objective function was the total power output. The design variables were the number of modules and the current in each control volume of the mesh. We also optimize directly the electrical topology of the system. A genetic algorithm was used to perform the optimizations. Complex optimal electrical topologies were achieved due to the non-uniform temperatures distributions in the heat exchanger.

1. Introduction

A thermoelectric generator is a device that converts thermal energy into electrical power. The problem that has plagued the industry for many years is the low conversion efficiency of thermoelectric generators. A lot of research is being conducted in that field with promising results. New developments of thermoelectric materials indicates that the efficiency of thermoelectric systems is likely to improve in the years to come [1], with the development of new materials and thin films with a higher figure of merit [2–5], thus making the use of thermoelectric generators more interesting in a variety of applications. Producing electrical power with a thermoelectric generator has many advantages. For example, it requires no moving parts, thus making it a very reliable system. Even though the conversion efficiency is low, the use of thermoelectric generator could be interesting for waste heat recovery, as there is no cost associated with the heat used for power production [6].

In the past, authors have developed models for thermoelectric generators while treating it as an irreversible heat engine [7]. Many others have explored the influence of various parameters on the performances of thermoelectric generators including the effect of multiple layers of modules [8,9]. Some research was also performed to optimize the geometry of the thermoelectric modules used in the generator [10]. While many of the works in that field were theoretical, some authors have studied experimentally real generators in order to validate their numerical models [11,12].

The ultimate goal of the development of such devices is to use them in various applications, in particular for waste heat recovery. For example, thermoelectric generators could be used in regions with unreliable electric supply when collecting heat from heating stoves [13]. Recently, Yu and Zaho have developed a numerical model for a thermoelectric generator within a parallel plate heat exchanger [14]. Also, some authors have explored the possibility of wearable thermoelectric generators for body-powered devices [15].

In this paper, we present a model and optimize the internal structure of a thermoelectric generator sandwiched in a crossflow heat exchanger. Crossflow heat exchangers are popular for waste heat recovery because of their low cost and easiness to manufacture and operate. First, we describe the model, along with a method to represent the various electrical connections between the thermoelectric modules. Then, we present the optimization results performed on the system for various operating conditions.

2. Modeling of a one-stage generator in a crossflow heat exchanger

In this section, we describe how the generator was modeled. We considered one layer of single-staged thermoelectric modules sandwiched between a hot and a cold flow in a crossflow heat exchanger, as seen in Fig. 1. The heat exchanger wall was divided in small control volumes (mesh) labeled in Fig. 1 by the index *i*. In our model, four temperatures in each control volume (T_H, T_C, T_1, T_2) need to be evaluated. The temperature must be evaluated in each fluid (i.e., T_H, T_C) and at the top and bottom surfaces of the thermoelectric modules (i.e., T_1, T_2). The fluid-to-fluid temperature

* Corresponding author. Tel.: +1 418 656 7829; fax: +1 418 656 7415.
E-mail address: Louis.Gosselin@gmc.ulaval.ca (L. Gosselin).

0196-8904/$ - see front matter © 2011 Elsevier Ltd. All rights reserved.
doi:10.1016/j.enconman.2011.02.019

Nomenclature

A	area, m^2
B	area to length ratio, m
C	conductance matrix
c_p	heat capacity, J/kg K
D	incidence matrix
F	heat capacity rate, W/K
I	current, A
k	thermal conductivity, W/mK
K	thermal conductance, W/K
L	length, m
m	number of thermoelectric modules
P	electrical power, W
q''	heat flux, W/m^2
R	electrical resistance, Ω
S	source term
T	temperature, K
u	velocity components, m/s
v	potential at each node, V
x, y, z	Cartesian coordinates, m

Greek symbols

α	Seebeck coefficient, V/K
ρ	density, kg/m^3
σ	electrical resistivity, Ω m

Subscript

C	relative to the cold fluid
H	relative to the hot fluid
1	relative to the surface with the hot fluid
2	relative to the surface with the cold fluid

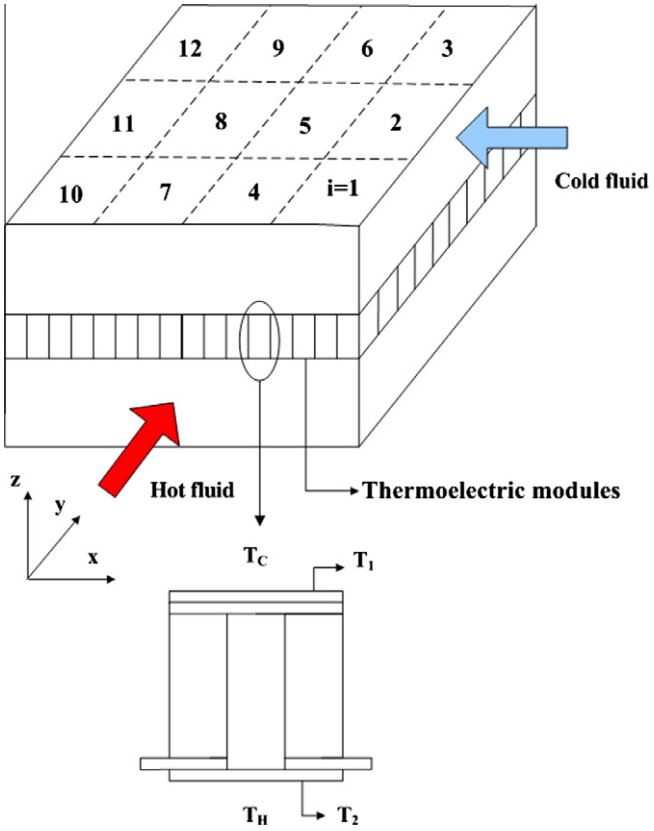

Fig. 1. Representation of a thermoelectric generator sandwiched in a crossflow heat exchanger with 12 control volumes.

difference in the heat exchanger will drive a current in the thermoelectric modules. The model evaluates the electrical power generated under various conditions for such a system.

In each control volume, the hot fluid transfers heat to the wall by convection and similarly the cold fluid receives heat from the wall. This yields the following equations for the local heat flux in the ith control volume.

$$q_{Hi} = h_{hi}(T_{Hi} - T_{1i})\Delta x\Delta y \tag{1}$$

$$q_{Ci} = h_{ci}(T_{2i} - T_{ci})\Delta x\Delta y \tag{2}$$

where h_{hi} and h_{ci} are the local convection coefficient on the hot and cold sides respectively. When fins are present in the heat exchanger, one would need to replace h in Eqs. (1) and (2) by $h\eta_f A_f/(\Delta x\Delta y)$ where η_f is the efficiency of the fin system, and $A_f/(\Delta x\Delta y)$ is the ratio of areas of the fin surface to the wall surface. Therefore, whenever we vary h later in this paper, this could be seen as equivalent to varying the design of the fin system.

The thermal conductance K and the electrical resistance R of the thermoelectric elements in the wall can be defined locally, and depend on the thermoelectric properties (thermal conductivity, k, and electrical resistivity, σ) and on the geometry of the legs,

$$K_i = k_n B_n + k_p B_p \tag{3}$$

$$R_i = \frac{\sigma_n}{B_n} + \frac{\sigma_p}{B_p} \tag{4}$$

where $B_n = A_n/L_n$ et $B_p = A_p/L_p$ are the n and p-legs cross-sectional area to length ratios (shape factor). A variable number of thermoelectric elements can be included in each control volume. We labeled m_i the number of modules in the ith control volume.

The local heat flux introduced in Eqs. (1) and (2) can be determined based on the geometry and properties of the modules [8],

$$q_{Hi} = \left(m\alpha I T_1 - \frac{mRI^2}{2} + mK(T_1 - T_2)\right)_i \tag{5}$$

$$q_{Ci} = \left(m\alpha I T_2 + \frac{mRI^2}{2} + mK(T_1 - T_2)\right)_i \tag{6}$$

where α is the Seebeck coefficient, and I is the electrical current flowing through the module. Eqs. (1), (2), (5) and (6) form a set of 4 equations with 6 unknowns (T_H, T_C, T_1, T_2, q_H, q_C) for each control volumes. Here, the current I has to be specified by the user and is not considered as an unknown. Specifying I is equivalent to specifying the load electrical resistance. Therefore, two additional relations between the six unknowns are required. These relations describe how the fluid temperatures vary according to the heat fluxes. Assuming that the velocities of the fluids are known, it is possible to perform an energy balance on each control volume. The heat removed from the hot stream will cool it. Therefore, a heat balance on the warm side yields, in the ith control volume:

$$q_{H_i} = F_H(T_{H,i-1} - T_{H,i}) \tag{7}$$

and similarly on the cold side

$$q_{C_i} = F_C(T_{C,i} - T_{C,i-discry}) \quad (8)$$

where $F = \rho c_p u$ is the heat capacity rate. These two equations provide the missing relations to close the problem invoked above. Eqs. (1)–(4) and (7), (8) can be rewritten in order to eliminate the heat fluxes and end up with 4 equations and 4 unknowns in each control volume (i.e., T_H, T_C, T_1, T_2). Once the temperatures are determined, the local heat flux (q''_H, q''_C) can be deduced using, for example, Eqs. (1) and (2). The local generation of thermoelectric power is the difference between heat fluxes q''_H and q''_C, and the total available power is obtained by integrating over the entire surface S of the generator,

$$P = \int\int_S (q''_H - q''_C) dS \quad (9)$$

The governing equations were discretized using the finite volume method, in order to be solved numerically. Our model was validated using two different limits. First, we validated the heat transfer portion of the code. When the output current is forced to zero, our model becomes a simple crossflow heat exchanger. Results provided by our model under that assumption were compared to those achieved with the NTU method. Details about this method can be found elsewhere [16]. We compared the temperature in each control volume for both methods (i.e. our code versus NTU method). Results showed that the maximal error between the two sets of results was of 0.3%, which means that our model is adequate under the assumptions mentioned above. In order to validate the thermoelectric part of the code, we reproduced the results obtained by Chen et al. [17] for a one-stage thermoelectric generator with fixed and uniform temperatures on both surfaces. Using the same size, operating conditions, and properties as that used in their article, we determined the resulting electrical power output versus the circulating current for various total numbers m of thermoelectric modules. We used high values of velocities and convection coefficients in order to achieve a uniform temperature on both sides of the heat exchanger as assumed in their work. The comparison is shown in Fig. 2 and proved our model correct.

3. Optimization procedure for distribution of current density and number of modules

The optimization problem consists in identifying the set of design variables that will maximize electrical power. We used the power output as the objective function rather than the efficiency because we assumed that the heat was free or at least cheap (i.e., waste heat). The geometry considered is shown in Fig. 1. The thermoelectric wall between the hot and cold fluids is separated in 10×10 control volumes (i.e., 100 control volumes). The parameters and physical properties that we considered for this test case are shown in Table 1. The generator was square-shaped. Two sets of design variables were considered: the currents (I) in each control volume and the number of thermoelectric modules (m) per control volume. Therefore, the total number of design variables is 200. The objective was to find the best combination of design variables that would maximize the electrical power output. The optimization strategy that was retained is a genetic algorithm (GA). We do not repeat here all the details relative to this approach. A recent review on their utilization in heat transfer is available [18]. The GA considered here used real numbers and was elitist. The current (I) variable was continuous while the number of modules per control volume (m) used integers. The main settings of the GA are summarized in Table 2. Convergence was declared when the improvement of the objective function was less than 0.1% during 250 consecutive generations. GAs being probabilistic methods, two runs with the same settings can potentially lead to two different results. Therefore, we performed four optimization runs with the GA for each test case considered in order to ensure the repeatability of the results. Only the best result among the four runs was retained and is presented here. I and m in each control volume are optimized as described in this section; the total current that will be delivered to the load does not need to be specified. Only the current in each control volume is determined. The determination of I_{tot} requires a knowledge of the way modules are electrically connected. This will be addressed later in Sections 5 and 6.

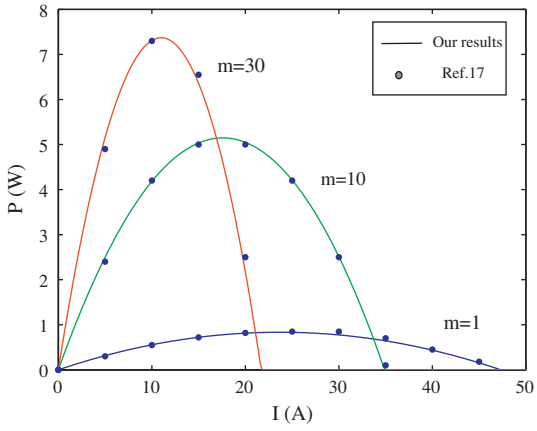

Fig. 2. Comparison of the power output determined from our model, and that reported by Chen et al. [17].

4. Optimized distribution of current density and number of modules

As stated before, we performed optimization runs for various sets of parameters. First, we fixed h to 1000 W/m^2 K, and ΔT_{in} to 400 K. While the ΔT_{in} (i.e., $T_{H_{in}} - T_{C_{in}}$) value may seem high enough to jeopardize the integrity of the modules, it is important to consider that wall-to-wall temperature difference is smaller and is actually what matters and influences the power output of the system. We then performed optimizations of I_i and m_i ($i = 1, 2, \ldots, 100$) for different heat capacity rates and heat exchanger side length L. We assumed that the cold heat capacity rate was equal to hot capacity rate (i.e., $F_C = F_H = F$). The influence of the heat capacity rate and of the side length on the maximized electrical power is represented in Fig. 3. Each point on that figure is the result of a full optimization with respect to the 200 design variables. We observed that the maximized electrical power output increases with the heat capacity rate. This is easily explainable by the fact that a

Table 1
Parameters and properties considered for the optimization of the generator sandwiched between crossflow streams [6,12].

Number of control volumes = 100 (10×10)
Seebeck coefficient (α) = 0.00022 V/K
Electrical resistivity of the legs (σ) = 0.000015 Ω m
Thermal conductivity of the legs ($k_n = k_p$) = 1.2 W/mK
Area to length ratio of the legs (B) = 0.01 m

Table 2
Main parameters used by the GA.

Number of individuals per population = 50
Mutation rate = 0.02
Crossover rate = 0.8
Elites proportion = 0.2

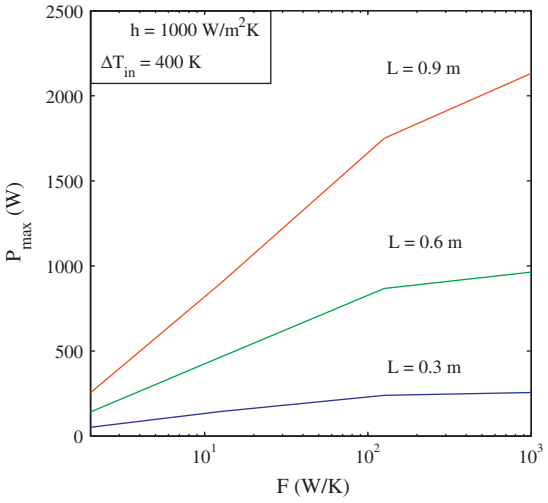

Fig. 3. Maximal electrical power output as a function of the entry velocity for various side lengths and heat capacity rates.

higher heat capacity rate increases the temperature difference in the thermoelectric modules. Ultimately, at infinitely large heat capacity rate and convection coefficient, the temperature drop in the modules would be at every location that of the fluids at the inlet of the heat exchanger (i.e., $\Delta T_i \rightarrow T_{H_{in}} - T_{C_{in}}$ when $F, h \rightarrow \infty$). If we look at the optimal current distributions in the generator, we see that the optimal currents are higher when the temperature difference in the thermoelectric modules is high and that it decreases with ΔT_i across the exchanger wall. This can be seen in Fig. 4a and c which shows the optimal current distribution and the actual temperature differences ($T_{1,i} - T_{2,i}$) for a given set of parameters. We can see that it would not be optimal to wire the control volumes in series nor in parallel because it is impossible to attain the desired currents in each control volume with those types of connections. On the other hand, the number of thermoelectric modules per control volume tends to increase as ΔT_i decreases across the exchanger, as revealed in Fig. 4b. The optimal current, module distribution, and temperature differences with a larger F are also shown in Fig. 5. Having a larger F means that the ΔT_i in each control volume will be larger than in the previous case. Fig. 5b shows that the number of modules per control volume is significantly larger than with a smaller F.

The influence of the heat exchanger size on the power output was also shown in Fig. 3 for three different side lengths (0.3 m, 0.6 m, and 0.9 m). The inlet cold-to-hot fluid temperature difference was fixed to 400 K, and h to 1000 W/m^2 K. We observed a great increase of the maximal electrical power with a growing heat exchanger side length. For each 0.3 m increment in the heat exchanger side length, the maximal electrical power almost doubles, but for each control volume the density of modules ($m''_{i_{opt}} = m_{i_{opt}}/\Delta x \Delta y$) remains nearly constant.

Next, we fixed the heat capacity rate to 12.6 W/K, the side length to 0.3 m, the ΔT_{in} to 400 K and then we performed optimizations for various convection coefficients (10^2, 10^3, 10^4, 10^5 W/m^2 K). As with the heat capacity rate, we noted an increase of the maximized electrical power output as the convection coefficient increases, see Fig. 6. This can be explained by the fact that a higher convection coefficient keeps the upper and lower side of the thermoelectric modules at a temperature close to the one of the fluid, thus increasing the overall temperature difference in the modules. It is important to remember that each point in Figs. 3 and 6 is in result of a full optimization of the 200 design variables mentioned above.

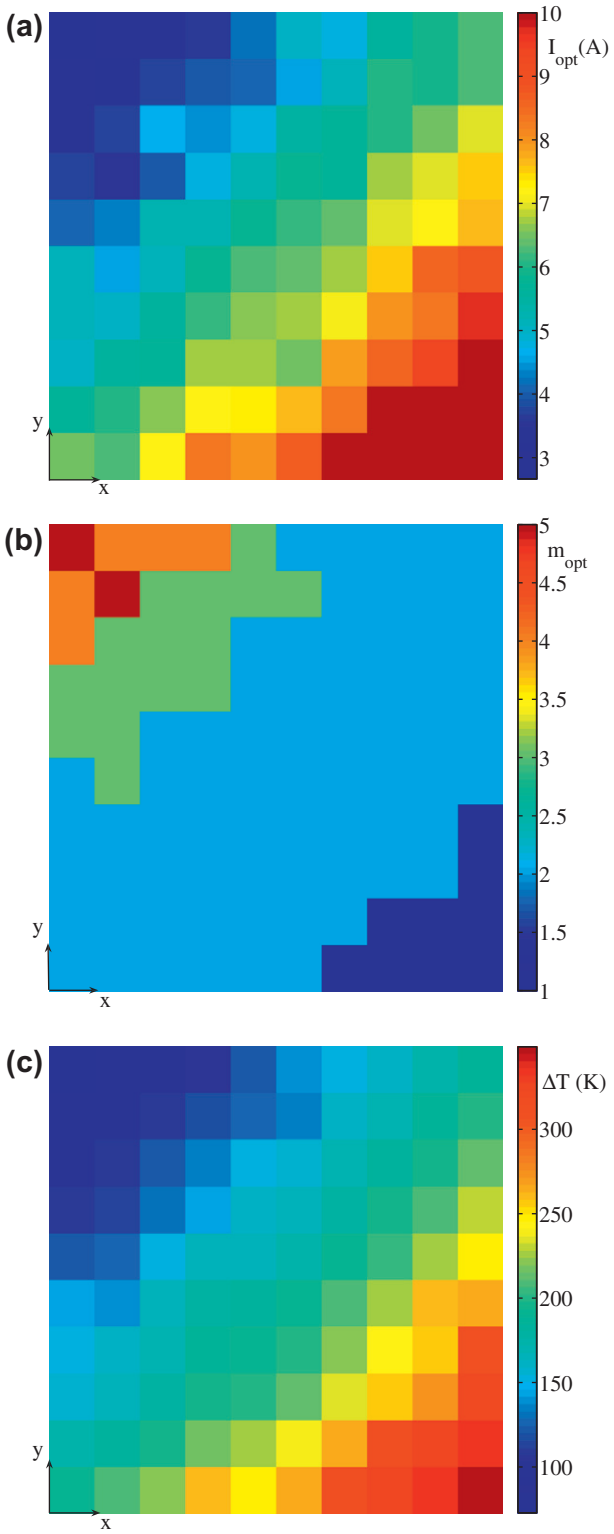

Fig. 4. Optimal solution for ΔT_{in} = 400 K, h = 1000 W/m^2 K, L = 0.3 m, and F = 1.26 W/K.

Next, we performed optimizations while varying the convection coefficient for various inlet temperature differences (ΔT_{in}). The results are presented in Fig. 6. The increase in the electrical power with ΔT_{in} is nearly linear. It is important to note that we did not consider a temperature limitation in the modules. In practice, all available thermoelectric modules on the market have a limitation

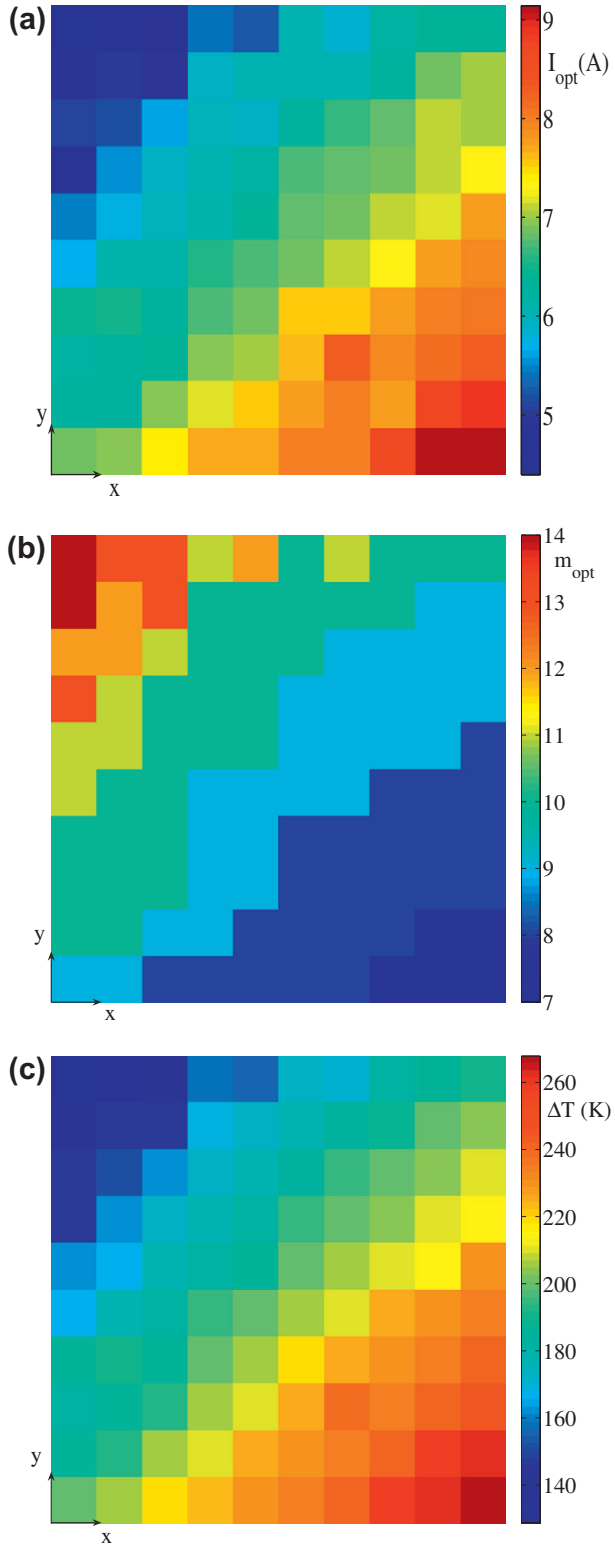

Fig. 5. Optimal solution for ΔT_{in} = 400 K, h = 1000 W/m^2 K, L = 0.3 m, and F = 12.6 W/K.

associated with a maximal operating temperature, which prevents them from degradation [19].

All results presented before were achieved assuming $F_H = F_C$ (i.e., equivalent heat capacity rates). As a final simulation, we performed the optimization (ΔT_{in} = 400 K, h = 1000 W/m^2 K, L = 0.3 m) but this time with an "unbalanced" heat exchanger with

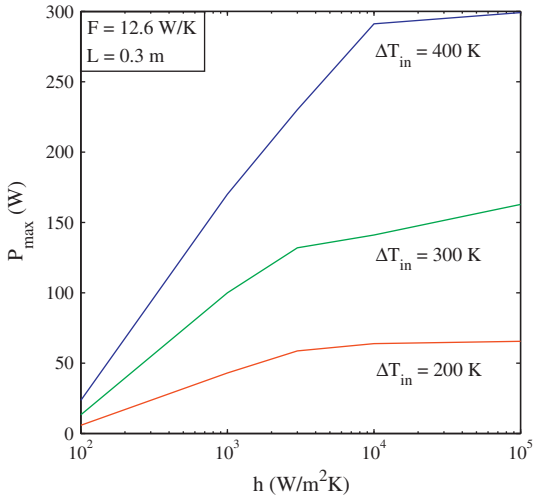

Fig. 6. Maximal electrical power output as a function of the convection coefficient for various cold-to-hot inlet fluids temperature differences.

F_{hot} = 12.6 W/K, and F_{cold} = 1260 W/K. The optimal results are presented in Fig. 7. Again, we see that the optimal parameters in the system are governed by the wall-to-wall temperature difference pattern ($T_{1,i} - T_{2,i}$). Because of the high heat capacity rate of the hot fluid, this side remained nearly at a uniform temperature.

5. Calculation of current distribution for a given electrical topology

In the previous sections, the total current into the load was not specified nor calculated. This requires the knowledge of the electrical topology (i.e., the way the modules are electrically connected). The current and module distributions could be optimized without this information as described before but the results of the optimization do not provide the electrical topology to actually use in order to achieve the desired current distribution. The next step is thus to determine this topology.

In this section, we explained how the topologies were represented and analyzed. In our problem, we will specify the total current that will be going out of the system into the load resistance (which is equivalent to specifying the value of the load resistance). Obviously, this is not necessarily the same amount of current that will be flowing in each control volume and will depend on the way each control volume is connected electrically to the other control volumes (electrical topology). Using linear algebra, it is possible to find the current in each control volume if the electrical topology is specified even if the connections are quite complex. This will allow us to see the effect of many wiring possibilities on the resulting electrical power. In this section, we explain briefly the fundamentals of this method based on graph theory, but more details can be found elsewhere [20]. In our problem, each control volume will contain two nodes, which will represent the electrical input and output of the control volume. In order to simplify the problem and diminish the number of electrical connection possibilities, we assume that each control volume can only be electrically connected to adjacent control volumes. Each electrical connection is an edge. The electrical topology can thus be represented by a graph. First, one must build the incidence matrix [20]. This matrix has a number of columns that is equal to the number of nodes and a number of rows equal to the number of edges (i.e., electrical connections). For a given geometry, the number of nodes will always be the same and the number of edges will be able to vary. Essentially, the incidence matrix is composed of 1,

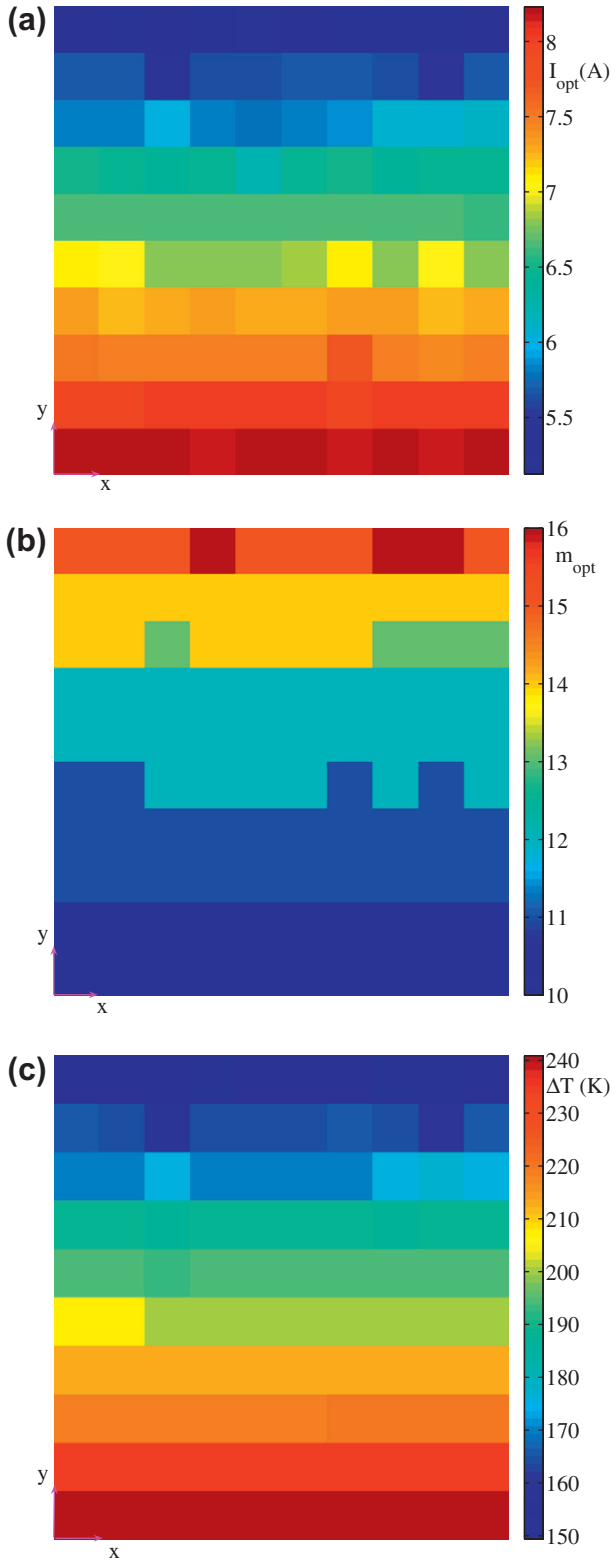

Fig. 7. Optimal solution for ΔT_{in} = 400 K, h = 1000 W/m^2 K, L = 0.3 m, F_{hot} = 12.6 W/K, and F_{cold} = 1260 W/K.

−1 and 0. For each edge, the value 1 will be given if the current goes into the node and the value −1 if the current goes out of the node. The remaining elements of the incidence matrix are 0. To summarize, each row can only have two non-zeros values. For example, if a system is composed of three nodes wired in series, the incidence matrix D could be the following:

$$D = \begin{bmatrix} -1 & 1 & 0 \\ 0 & -1 & 1 \end{bmatrix} \tag{10}$$

The next step is to build the conductance matrix. This matrix is diagonal and the values on the diagonal represent the conductance associated with each edge of the system. Essentially, two types of edges are present: (i) connection between adjacent control volumes, and (ii) connection between the input and output of a control volume. The edges between the input and output of a control volume will be the inverse of the resistances evaluated with Eq. (4) and vary with the number of modules in the control volume. The other conductance values are associated with the links between the control volumes. Their conductance will be considered infinite, i.e., that their resistance is negligible in front of that of the modules. For our previous example, Eq. (10), the conductance matrix C could be:

$$C = \begin{bmatrix} 1/R_1 & 0 \\ 0 & 1/R_2 \end{bmatrix} \tag{11}$$

Only one matrix remains to be built before we can solve the problem of determining the current in each control volume. It is the source matrix (S). This is a column matrix which length equals the number of nodes in the system. The only non-zero elements in this matrix correspond to values of current coming from outside sources flowing in the system or leaving the system. When all matrices have been built, one must solve a linear equation system in order to determine the potential value at each node. The equation is the following:

$$D^T C D v = S \tag{12}$$

where v represents the resulting potential at each node. Finally, one last step remains to determine the current in each electrical link:

$$I = -CDv \tag{13}$$

This procedure allows us to determine the current in each branch of the system for various topologies (I is a vector here with as many elements as there are edges). This representation will be useful to optimize module connections in the system under various operation conditions.

6. Optimization procedure for the electrical topology

As shown before (Figs. 4, 5 and 7), the optimal current distribution in the heat exchanger wall is non-uniform. Therefore, connecting the modules in series or in parallel is not the best option to maximize the electrical power output. This raises the question of how we should electrically connect each control volume in order to achieve the desired current distributions such as that determined in Section 4. In order to optimize the electrical topology, we used graph theory and linear algebra, as described in Section 5, to simulate various topologies in order to find the one which approaches at best the optimal solution found in Section 5.

The control volume was represented by an input and an output node. The input and output of a control volume were only connected together by one link which represented the thermoelectric modules in the control volume. In other words, each input current going into the control volume was associated to the input node and every outgoing current was associated with the output node. To simplify our analysis, we restricted the possibilities of connections only to neighboring control volumes. In other words, a control volume could only be connected electrically to its four adjacent neighbors. This means that a maximum of 15 possible sets of connections per control volume are possible. For each control volume, we only consider the currents flowing into its input node. Considering the currents leaving through the output node is not

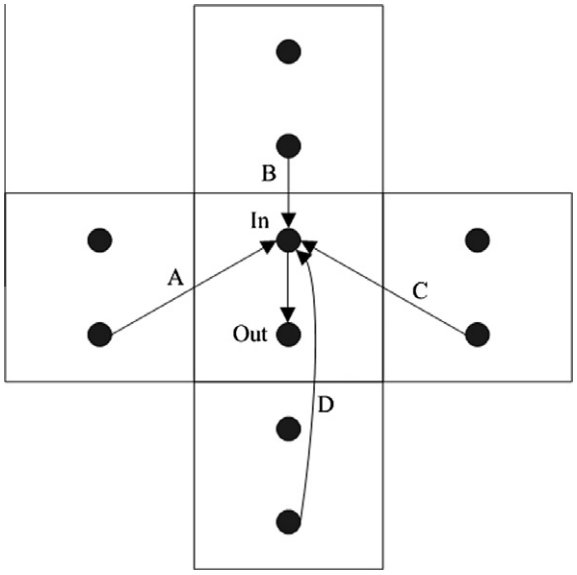

Fig. 8. Schematic of the possible connection between adjacent control volumes.

useful as it is included as an input for the control volume(s) it is connected to. Consider the central control volume in Fig. 8 and its four adjacent neighbors. We call A a connection with the left-hand side neighbor only, and so on. The 15 possible sets of connections are thus: A, B, C, D, AB, AC, AD, BC, BD, CD, ABC, ABD, BCD, ABCD. The label AB means that the links A and B in Fig. 8 are present, but not the links C and D. Also, all the control volumes touching the bottom edge of the heat exchanger could be connected to an external node from which the overall input current to the system flows. The same procedure was used for the topmost control volumes in the heat exchanger, but for the total output current. In our approach, each set of connection was represented by an integer which was then decoded by the program and transformed into edges. For example, a connection A was attributed the integer 1, a connection set AB, 2, and so on for the other 15 possible connections. Once the electrical connection topology is entirely mapped, it becomes possible to find the value of the current in each control volume as previously described. In order to do that, we must specify the total current which is entering the system. In fact, the total current will become a design variable when we design the topology. It is equivalent to determine the optimal load resistance.

In our analysis, we assumed that the electrical resistance of the wires was negligible so that only the resistance in the thermoelectric modules needed to be considered. We used a genetic algorithm to maximize the electrical power output while changing only how the system is electrically connected as well as the overall current. We took a case in which we knew the optimal current distribution (see Section 5), and we fixed the number of modules in our model with the optimal parameters calculated before (Section 5) to see if we could attain the optimized current distribution by varying the topology.

We had two types of design variables: the connections in each of the 100 control volumes, and the total current entering the system. For each control volume, the connection variable was represented by an integer. Each number was then decoded by the program and transformed into an edge. The total current variable (I) was a real continuous number. Therefore, the total number of design variables was 101. We used the same algorithm parameters as those shown in Table 2. The genetic algorithm was stopped when the objective function changed by less than 0.1% during 5000 consecutive generations.

7. Results for the optimization of the electrical topologies

For this part, we used the properties shown in Table 1 and we fixed h to 1000 W/m^2 K, ΔT_{in} to 400 K, the side length to 0.3 m, and the heat capacity rate 12.6 W/K. As stated before, we tried to find the electrical topology that approaches at best the optimal solution found in Section 5 (i.e. Fig. 4). The maximal power output found in Section 4 (i.e., without determining the actual topology) for this case was of 145.7145 W. After approximately 7000 generations with the GA, the topology shown in Fig. 9 was produced. To facilitate the interpretation of the drawing, the input and output nodes of a given control volume were grouped as one node, which explains the presence of a lone double-arrow in some control volumes. The electrical power output for the presented design is of 145.6689 W, which is 0.03% short of the optimal solution of Fig. 4a. As we thought, the topology found by the GA is far from intuitive and very complex. It would be logical to assume that other nearly optimal solutions are possible including some that corresponds to symmetry of the design of Fig. 9. The solution found can also be compared to solutions found while using simpler electrical topology (i.e., series and parallel). In order to do so, we performed optimizations with the GA using a given electrical topology. Our two design variables were the number of modules in each control volume and the total input current in the system. We performed optimizations for the cases where the control volumes were connected in series and in parallel. The results are presented in Table 3. The lowest maximal electrical power output was achieved when all the control volumes were connected in series. Even if our lowest result came from this electrical topology, it is only 1% below the maximal possible value. The parallel topology was slightly better than in series, because the system had a little

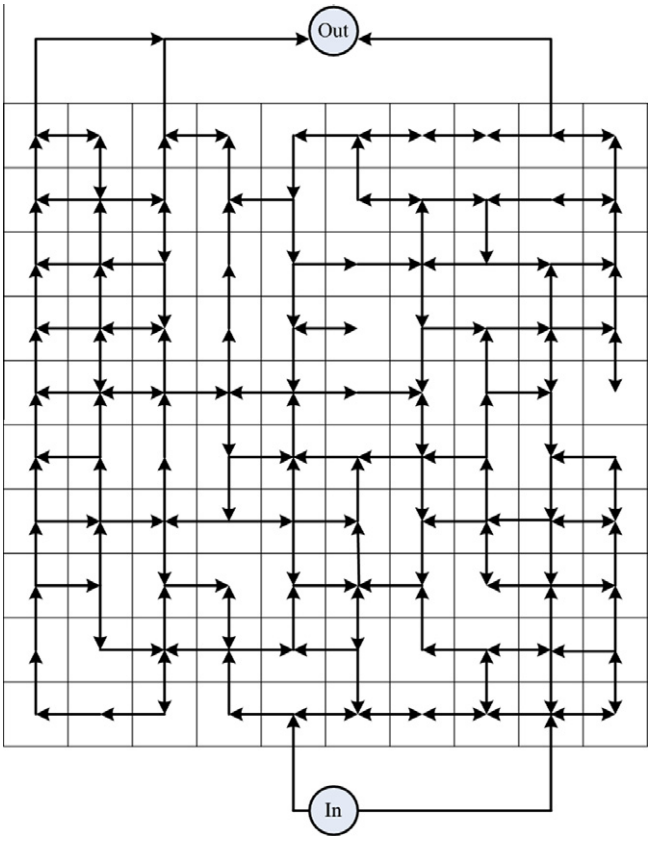

Fig. 9. Optimal electrical topology that maximizes the electrical power output for the case of Fig. 3a.

Table 3
Comparison of the maximal electrical power output as a function of the electrical topology.

Type of connections	Maximal electrical power output (W)
Optimal solution (Fig. 3a)	145.7145
Topology of Fig. 8	145.6689
Parallel	144.8372
Series	143.9295

more room to adapt and was closer to the optimal current distribution. Finally, the topology found in Section 5 provided the best electrical power output among all others. While the improvement from the other cases is relatively modest in this case, it could vary depending on operating conditions for which non-uniform temperature distributions prevail. Our method showed that an optimized electrical topology is beneficial in a crossflow heat exchanger in order to achieve the best electrical power output, even though, for the test case tester, the gain of power is relatively weak.

8. Conclusion

In this paper, we propose a design procedure for a thermoelectric generator sandwiched in a crossflow heat exchanger. Such heat exchangers are routinely used to recuperate waste heat in many applications. The approach determines how many modules should be used and how to position them in the wall. This was represented by the design variable m. The optimization procedure also determines the optimal current distribution in the heat exchanger wall. We relied on genetic algorithms to perform the optimization.

The second step that we took was to optimize directly the electrical topology, which was represented by incidence and conductance matrices. The optimized topologies achieved were slightly better than parallel or series configurations.

Future work could focus on designing the heat exchanger channel (e.g., fins, etc.) simultaneously with the thermoelectric wall to enhance performance. In that case, we could include the non-uniform distribution of the convection coefficient in the approach. Multi-stages thermoelectric designs could also be optimized with a similar procedure. Furthermore, constraints such as cost, weight, temperatures could be included in the approach.

Acknowledgement

The authors' work was supported by the Natural Sciences and Engineering Research Council of Canada (NSERC).

References

[1] Venkatasubramanian R, Siivola E, Colpitts T, O'Quinn B. Thin-film thermoelectric devices with high room-temperature figures of merit. Nature 2001;413:597–602.
[2] Yu C, Chau KT. Thermoelectric automotive waste heat energy recovery using maximum power point tracking. Energy Convers Manage 2009;50:1506–12.
[3] Zeng G, Bahk J, Bowers JE, Lu H, Gossard A, Singer SL, et al. Thermoelectric power generator module of 16 × 16 Bi_2Te_3 and 0.6% ErAs:(InGaAs)1−x(InAlAs)x segmented elements. Appl Phys Lett 2009;95:083503.
[4] André C, Vasilevskiy D, Turenne S, Masut RA. Extruded bismuth-telluride-based n-type alloys for waste heat thermoelectric recovery applications. J Elect Mat 2009;38:1061–7.
[5] Schilz J, Helmers L, Müller WE, Niino M. A local criterion for the composition of graded thermoelectric generators. J Appl Phys 1998;83:1150–2.
[6] Wu C. Analysis of waste-heat thermoelectric power generators. Appl Therm Eng 1996;16:63–9.
[7] Ozkaynak S, Gotkun S. Effect of irreversibilities on the performance of a thermoelectric generator. Energy Convres Manage 1994;35:1117–21.
[8] Chen L, Li J, Sun F, Wu C. Performance optimization of a two-stage semiconductor thermoelectric-generator. Appl Energy 2005;82:300–12.
[9] Yu J, Zhao H, Xie K. Analysis of optimum configuration of two-stage thermoelectric modules. Cryogenics 2007;47:88–93.
[10] Riffat SB, Ma X. Optimum selection (design) of thermoelectric modules for large capacity heat pump applications. Int J Energy Res 2004;28:1231–42.
[11] Yamashita O, Odahara H, Satou K. Energy conversion efficiency of a thermoelectric generator under the periodically alternating temperature gradients. J Appl Phys 2007;101:023704.
[12] Niu X, Yu J, Wang S. Experimental study on low-temperature waste heat thermoelectric generator. J Power Sources 2009;188:621–6.
[13] Nuwayhid RY, Rowe DM, Min G. Low cost stove-top thermoelectric generator for regions with unreliable electricity supply. Renew Energy 2003;28:205–22.
[14] Yu J, Zaho H. A numerical model for thermoelectric generator with the parallel-plate heat exchanger. J Power Sources 2007;172:429–34.
[15] Leonov V, Vullers RJM. Wearable thermoelectric generators for body-powered devices. J Elect Mater 2009;38:1491–8.
[16] Incropera FP, Dewitt DP, Bergman TL, Lavine AS. Fundamentals of heat and mass transfer. 6th ed. John Wiley & Sons; 2007. p. 669.
[17] Chen L, Gong J, Sun F, Wu C. Effect of heat transfer on the performance of thermoelectric generators. Int J Therm Sci 2001;41:95–9.
[18] Gosselin L, Tye-Gingras M, Mathieu-Potvin F. Review of genetic algorithms utilization in heat transfer problems. Int J Heat Mass Transfer 2009;52:2169–88.
[19] Federici JA, Norton DG, Bruggemann T, Voit KW, Wetzel ED, Vlachos DG. Catalytic microcombustors with integrated thermoelectric elements for portable power production. J Power Sources 2006;161:1469–78.
[20] Strang G. Introduction to linear algebra. Wellesley-Cambridge Press; 1993. p. 337.